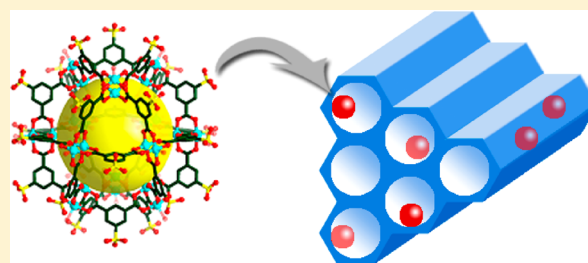


## Confinement of Metal–Organic Polyhedra in Silica Nanopores

Lin-Bing Sun,<sup>†</sup> Jian-Rong Li,<sup>\*,†,‡</sup> Weigang Lu,<sup>†</sup> Zhi-Yuan Gu,<sup>†</sup> Zhiping Luo,<sup>§</sup> and Hong-Cai Zhou<sup>\*,†</sup><sup>†</sup>Department of Chemistry, Texas A&M University, College Station, Texas 77842-3012, United States<sup>‡</sup>College of Environmental and Energy Engineering, Beijing University of Technology, Beijing 100124, P. R. China<sup>§</sup>Microscopy and Imaging Center, Materials Science and Engineering Program, Texas A&M University, College Station, Texas 77843, United States

## S Supporting Information

**ABSTRACT:** Metal–organic polyhedra (MOPs) have been incorporated into silica nanopores for the first time. Three MOPs with identical geometries but different ligand functionality (namely *tert*-butyl, hydroxyl, and sulfonic groups) were employed. A typical mesoporous silica, SBA-15, with a two-dimensional hexagonal pore regularity was used as the host. In comparison with bulk MOPs, which prefer to aggregate, MOPs confined in silica nanopores can be well dispersed, making the active sites and pores in the MOPs accessible. These dispersed MOPs showed apparently superior H<sub>2</sub> adsorption capacity in comparison with aggregated bulk MOPs. Moreover, the thermal stability of the MOPs was enhanced upon their confinement in silica nanopores.



## ■ INTRODUCTION

Metal–organic polyhedra (MOPs) are discrete molecular architectures constructed via the coordination of metal ions and organic linkers. Because of their intriguing structures, relevance to biological self-assembled systems, and diverse potential applications (such as in guest molecule inclusion, sensing, and catalysis), MOPs have attracted great attention in the past decade.<sup>1</sup> It is known that activation (i.e., the removal of guest molecules to get accessible pores) is necessary for both MOPs and metal–organic frameworks (MOFs) prior to use in catalytic and adsorptive processes.<sup>2</sup> For uniformly constructed MOFs, the accessibility of active sites is improved after activation, and their interconnected channels and cavities allow guest molecules to shuttle. However, unlike MOFs, MOP molecules tend to aggregate after activation, which results in the blockage of active sites by adjacent MOP cages.<sup>3</sup> This weakens the performance of MOPs severely, and in some cases, MOP materials do not exhibit any visible adsorptive or catalytic activity at all.<sup>4</sup> Therefore, the development of an effective method of dispersing MOP molecules in the solid state is extremely desirable.

Another group of porous materials that have received considerable interest are mesoporous silicas. Since the discovery of mesoporous silica M41S, an incredible degree of control over silica with various pore symmetries (e.g., hexagonal, cubic, and lamellar) has been achieved.<sup>5</sup> These silica materials contain ordered pores on a nano scale (with the pore size being tunable from 2 to 50 nm), which makes them valuable as supports for dispersing a variety of guests ranging from metal and oxide nanoparticles to peptide and drug macromolecules.<sup>6</sup> Mesoporous silicas as well as zeolites have also been used as hosts for supramolecular organization of various organometallic

compounds (e.g., trimethyltriazacyclononane manganese, nickel polyamine, and hexacarbonylchromium complexes), which is known in the realm of intramessoporous silica chemistry and intrazeolite chemistry.<sup>7</sup> Taking into account that MOPs have molecular dimensions of several nanometers, silica nanopores should be an ideal accommodation for MOP molecules. If MOPs are introduced into silica nanopores, aggregation that takes place for bulk MOP molecules may be avoided, and the active sites may become accessible. Moreover, because of the special microenvironment in silica nanopores, the confinement of MOPs would be expected to enhance the stability of MOP molecules. In the meanwhile, these loaded MOPs could also modify the mesopores of silica to give unique properties and functions desirable for applications in adsorption and catalysis. To the best of our knowledge, however, the confinement of MOPs in mesoporous silicas, or even in other mesoporous materials, has not been reported to date.

Herein we report the confinement of MOP molecules in silica nanopores for the first time. By taking advantage of the solubility of MOPs and the interaction between MOPs and mesoporous silica, we have incorporated several precisely selected MOPs into silica nanopores to fabricate a new type of composite, namely, mesoporous silica-confined MOPs. Both the symmetry of the silica mesopore and the molecular structure of the MOP are well-maintained in the composite. The dispersibility of MOPs in silica nanopores is greatly improved, making the active sites in the MOPs accessible. These dispersed MOPs show apparently superior H<sub>2</sub> adsorption capacity in comparison with aggregated bulk

Received: July 1, 2012

Published: August 31, 2012

MOPs. Furthermore, the confinement of MOPs in nanopores also enhances the thermal stability of the MOP molecules.

## EXPERIMENTAL SECTION

**Chemicals.** Copper(II) acetate monohydrate [ $\text{Cu}_2(\text{OAc})_4 \cdot 2\text{H}_2\text{O}$ ], *N,N*-diethylformamide (DEF), *N,N*-dimethylacetamide (DMA), and three ligands, 5-*tert*-butyl-1,3-benzenedicarboxylic acid ( $\text{H}_2\text{L1}$ ), 5-hydroxy-1,3-benzenedicarboxylic acid ( $\text{H}_2\text{L2}$ ), and 5-sulfo-1,3-benzenedicarboxylic acid monosodium salt ( $\text{NaH}_2\text{L3}$ ) were purchased from Alfa Aesar Chemicals. Hydrochloric acid (HCl), dichloromethane ( $\text{CH}_2\text{Cl}_2$ ), methanol, and ethanol were purchased from BDH Chemicals. The triblock copolymer P123 ( $\text{EO}_{20}\text{PO}_{70}\text{EO}_{20}$ ) and tetraethylorthosilicate (TEOS) were obtained from Sigma-Aldrich. All of the starting materials were used without further purification.

**Materials Synthesis.** MOPs were synthesized according to our reported method.<sup>3a</sup> A DMA solution (20 mL) of 5-*tert*-butyl-1,3-benzenedicarboxylic acid (445 mg) was mixed with a DMA solution (20 mL) of  $\text{Cu}_2(\text{OAc})_4 \cdot 2\text{H}_2\text{O}$  (400 mg) in a glass vial (50 mL) and stirred for 30 min at room temperature. Next, 10 mL of MeOH was added to this solution, and the vial was then allowed to stand at room temperature. After 20 days, homogeneous dark-blue block crystals of the MOP [ $\text{Cu}_{24}(\text{L1})_{24}\text{S}_{24}$ ] $\cdot x\text{S}$  (**1**), where S represents a solvent molecule, were harvested (Figure 1a). Similarly, the MOPs

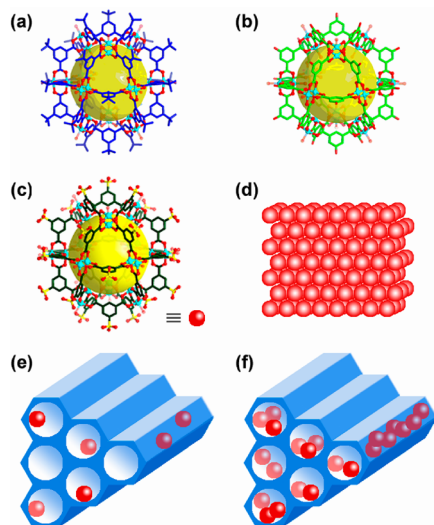


**Figure 1.** Schematic illustrations of (a–c) the crystal structures of (a) MOP 1, (b) MOP 2, and (c) MOP 3; (d) aggregated bulk MOP 3 molecules; and (e, f) MOP 3 dispersed in silica nanopores at (e) low and (f) high loadings. Color scheme: Cu atoms, cyan; O atoms, red; S atoms in MOP 3, yellow. The large yellow spheres represent the free space inside the molecular cages.

[ $\text{Cu}_{24}(\text{L2})_{24}\text{S}_{24}$ ] $\cdot x\text{S}$  (**2**) and  $\text{Na}_6\text{H}_{18}[\text{Cu}_{24}(\text{L3})_{24}\text{S}_{24}] \cdot x\text{S}$  (**3**) were synthesized using 5-hydroxy-1,3-benzenedicarboxylic acid and 5-sulfo-1,3-benzenedicarboxylic acid monosodium salt, respectively [see the Supporting Information (SI) for details].

SBA-15 mesoporous silica was prepared according to the literature.<sup>8</sup> In a typical synthesis, 2 g of P123 was dissolved in 60 g of 2 M HCl aqueous solution with stirring at 40 °C. Next, 4.25 g of TEOS was added to the homogeneous solution, which was then stirred at this temperature for 24 h. Finally, the mixture was heated to 100 °C and held at this temperature for 24 h under static conditions. The as-prepared sample was recovered by filtration, washed with water, and air-dried at room temperature. The removal of template was carried out by extraction with ethanol for 3 days.

Samples of the composites (denoted as  $\text{MnS}$ ,  $n = 1–3$ ) were prepared by impregnation. In a typical synthesis, MOP 3 (40 mg) was dissolved in 10 mL of methanol, after which 60 mg of SBA-15 was added. The mixture was stirred for 4 h, and then the methanol was

removed by evaporation at 80 °C, affording a blue solid that was denoted as M3S-0.4, where 0.4 represents the mass fraction of MOP 3 in the sample. In a similar process, M3S samples with different MOP 3 contents, denoted as M3S-0.1, M3S-0.2, M3S-0.3, and M3S-0.6, were synthesized. The Cu contents of the samples were measured by inductively coupled plasma atomic emission spectrometry (ICP-AES). The samples M3S-0.1, M3S-0.2, M3S-0.3, M3S-0.4, and M3S-0.6 possessed Cu contents of 0.21, 0.46, 0.74, 0.90, and 1.36 mmol  $\text{g}^{-1}$ , respectively, in good agreement with the theoretical values. A similar process was adopted for the preparation of  $\text{M3S}(\text{CH}_2\text{Cl}_2)$ , except that in the process of impregnation,  $\text{CH}_2\text{Cl}_2$  (in which MOP 3 is insoluble) was used as the solvent instead of methanol. The evaporation of  $\text{CH}_2\text{Cl}_2$  was performed at 40 °C. The samples M1S, M1S( $\text{CH}_2\text{Cl}_2$ ), M2S, and M2S( $\text{CH}_2\text{Cl}_2$ ) were prepared in a similar fashion (see the SI for details).

**Instrumentation.** Powder X-ray diffraction (PXRD) patterns of the materials were recorded using a Bruker D8-Focus Bragg–Brentano X-ray powder diffractometer equipped with a Cu-sealed tube ( $\lambda = 1.54178 \text{ \AA}$ ) at 40 kV and 40 mA. Transmission electron microscopy (TEM) and energy-dispersive X-ray (EDX) analyses were performed using a FEI Tecnai G2 F20 electron microscope operated at 200 kV. Field-emission scanning electron microscopy (SEM) was performed using a Hitachi-4900 electron microscope. Thermogravimetry analysis (TGA) was conducted on a Shimadzu TGA-50 analyzer. About 10 mg of sample was heated from room temperature to 600 °C in a  $\text{N}_2$  flow (25 mL  $\text{g}^{-1}$ ). Fourier transform IR measurements were performed on a Shimadzu IRAffinity-1 spectrometer.  $\text{N}_2$  and  $\text{H}_2$  adsorption isotherms were measured using a Micromeritics ASAP 2020 system at 77 K. Cu contents were measured by ICP-AES (Optima 2000DV, PerkinElmer).

## RESULTS AND DISCUSSION

The first MOP used in the present study was MOP 3. Structurally, MOP 3 has a cuboctahedral geometry when the 12  $\text{Cu}_2$  units are viewed as vertices and the ligands are viewed as edges (Figure 1c). This MOP is soluble in methanol, which plays a crucial role in its incorporation into silica nanopores, as discussed below. SBA-15, a typical mesoporous silica with the two-dimensional hexagonal pore regularity of the  $P6mm$  space group, was employed as the support.<sup>8</sup> The pore size of SBA-15 is 97 Å (Figure 2 and Table S1 in the SI), which is appropriate for the accommodation of molecules of MOP 3, which have a diameter of 29 Å. A wet-impregnation approach was used to incorporate different amounts of MOP 3 into SBA-15 nanopores after 3 was dissolved in methanol.

The  $\text{N}_2$  adsorption–desorption isotherm for the SBA-15 parent material is of type IV with an H1 hysteresis loop, which is the typical characteristic of materials with cylindrical mesopores (Figure 2).<sup>9</sup> Activated bulk MOP 3 exhibits negligible  $\text{N}_2$  uptake even at 77 K (Figure S2 in the SI), probably due to the aggregation of MOP molecules, as shown schematically in Figure 1d. Interestingly, the incorporation of MOP 3 into SBA-15 results in an obvious change in the hysteresis shapes of the isotherms. The hysteresis remains open up to a relative pressure of 0.5, which is apparently delayed in contrast with the original one, which closed at a relative pressure of 0.7. Moreover, increasing the amount of MOP 3 in the composite enhances the hysteresis at low pressures. These results demonstrate that the MOP molecules are located inside the mesopores of SBA-15. Otherwise, if the MOPs were located outside the mesopores, the overall uptake would decrease while the hysteresis shape would not change. The pore size distribution gives further evidence of the location of MOP molecules inside the mesopores (Figure 2; also see Figure S2 and Table S1 in the SI). A monomodal pore size distribution at 97 Å is observed for parent SBA-15. The introduction of MOPs

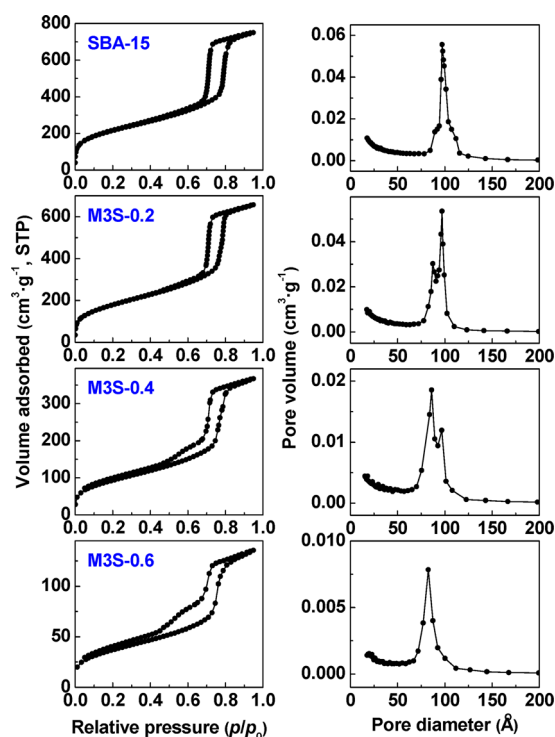


**Figure 2.** N<sub>2</sub> adsorption–desorption isotherms and pore size distributions for SBA-15 and M3S samples at 77 K. Pore size distributions were calculated from the adsorption branches using the Barrett–Joyner–Halenda (BJH) method.

leads to the appearance of a new pore size distribution at 86 Å. Importantly, with increasing MOP content in the sample, the number of 86 Å pores increases while the number of 97 Å pores declines progressively. Eventually, the 97 Å pores disappear, and a monomodal pore size distribution at 86 Å is detected for the sample M3S-0.6. According to this changing trend, we consider that only part of pore walls are occupied by MOPs for samples with low MOP loading, while more of the walls are occupied with increasing MOP content. Therefore, the appearance of a monomodal pore size distribution at 86 Å may mean the formation of a MOP monolayer on the walls of the mesoporous silica.

Figure 3 presents TEM images taken with the beam direction parallel to the pore channels of SBA-15. The hexagonally ordered pore structure can be distinguished in all of the M3S samples and is comparable to that in the parent SBA-15. Moreover, images taken with the beam direction perpendicular to the pore channels show large-area ordered mesopores (Figure S3 in the SI). These results suggest that the pore regularity is well-preserved after MOP incorporation. Figure S4 in the SI shows the low-angle PXRD patterns. The samples containing MOPs display diffraction peaks similar to those of the parent SBA-15, indicating that the ordered mesostructure is preserved and confirming the TEM results. In addition, the diffraction peaks become weaker with increasing MOP content because the introduction of the guest lowers the scattering contrast between the pore walls and the pore space. Because metal–organic systems are generally sensitive to electron beams, it is hard to discern the MOPs directly from the TEM images. Fortunately, EDX analysis verified the presence of MOPs in the samples. Copper and sulfur from the MOPs were detected in the M3S samples, as shown in Figure S5 in the SI. Also, the intensities of both signals increased with increasing

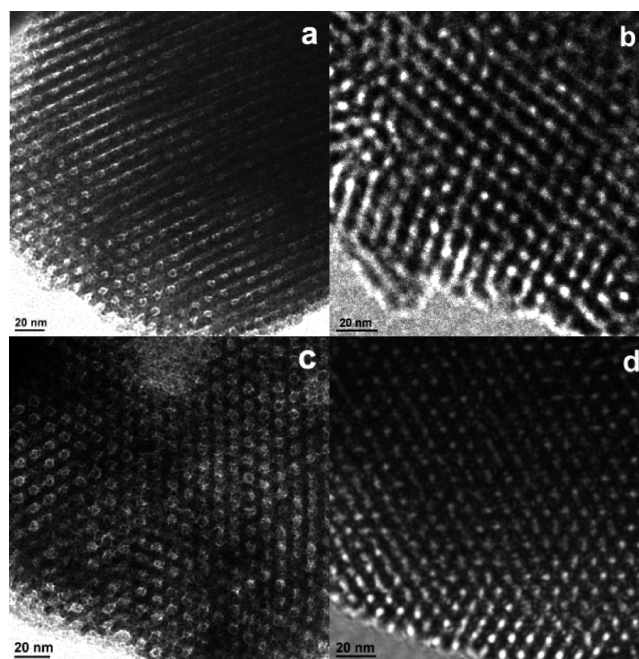


**Figure 3.** TEM images of (a) SBA-15, (b) M3S-0.2, (c) M3S-0.4, and (d) M3S-0.6 samples.

MOP content in the composite. The IR spectra of samples were also recorded and are shown in Figure S6 in the SI. All of the vibrational bands assigned to MOP 3 are observable for the M3S samples,<sup>3a</sup> and the peak intensities keep increasing with increasing MOP content, in good agreement with the EDX results. SEM images of different samples were also recorded. As shown in Figure S7 in the SI, the morphology of the parent SBA-15 was well-preserved after loading of MOPs. Moreover, the elemental maps show that copper and sulfur are well-distributed over the whole sample (Figure S8 in the SI), indicating the homogeneity of the MOP cages in the silica nanopores.

The PXRD pattern of SBA-15 exhibits a single broad diffraction peak ascribed to amorphous silica (Figure 4). The

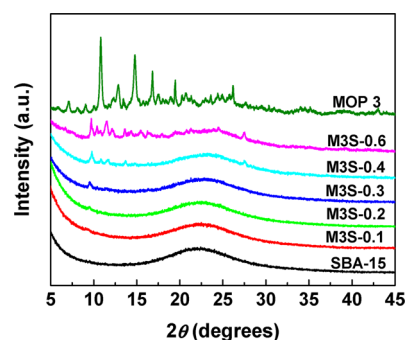


**Figure 4.** PXRD patterns of SBA-15, MOP 3, and M3S samples.

samples M3S-0.1 and M3S-0.2 show patterns almost the same as that of SBA-15, indicating that MOP 3 molecules may be well-dispersed in the silica nanopores, as shown schematically in Figure 1e. Nevertheless, some new diffraction peaks become visible upon further enhancement of the MOP loading. A series of diffraction peaks can be clearly identified in the PXRD pattern for sample M3S-0.6. Interestingly, these peaks are inconsistent with those of bulk MOP 3 crystals. These results



suggest the aggregation of MOP molecules in the nanopores with increasing loading amount (Figure 1f). However, the aggregation state of MOPs in silica nanopores is apparently different from that of bulk MOPs because of the confinement effect.

TGA showed that the decomposition of MOP 3 begins at 318 °C (Figure 5). However, when the MOPs are confined in

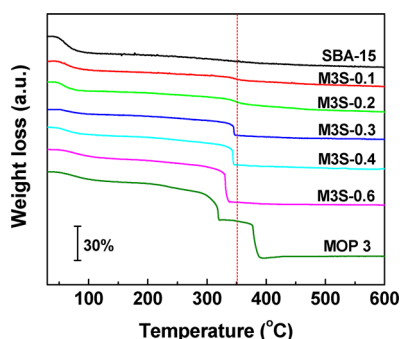


Figure 5. TGA curves of SBA-15, MOP 3, and M3S samples.

silica nanopores, the decomposition temperature increases to 331 °C for M3S-0.6. Interestingly, with decreasing MOP content, the decomposition temperature keeps increasing to 343 °C (M3S-0.4), 346 °C (M3S-0.3), and 350 °C (M3S-0.1 and M3S-0.2). It is clear that the MOP exhibits improved thermal stability within the confined space. The stability is also dependent on the extent of dispersion of the MOPs in the nanopores, with higher dispersion resulting in better stability. The interaction between MOP molecules and the interior surface of the silica should be responsible for the improvement in the stability. In addition to SBA-15 with the pore size of 97 Å, two hosts with pore sizes of 77 and 42 Å were also employed, and the stability of the resulting samples was investigated (Figure S9 in the SI). The decomposition temperatures of the MOPs for the hosts with pore sizes of 77 and 42 Å are 336 and 331 °C, respectively, indicating that the stability of the MOPs declines with decreasing pore size of the hosts. Nevertheless, MOPs dispersed in silica nanopores exhibit higher stability despite different pore sizes of the hosts.

Figure 6 presents the H<sub>2</sub> adsorption capacities of MOPs with different dispersion states. For bulk MOP 3, a negligible amount of H<sub>2</sub> is adsorbed because of the aggregation of MOP molecules and the blockage of open windows or active sites by

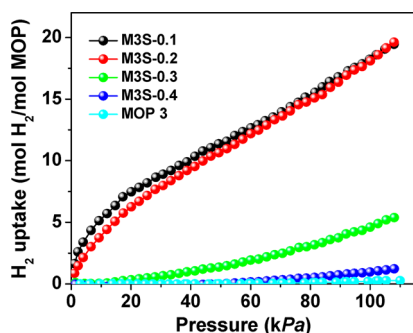


Figure 6. H<sub>2</sub> adsorption capacities of M3S and MOP 3 samples at 77 K. The adsorption capacities of M3S samples (mol of H<sub>2</sub>/mol of MOP) were calculated by subtracting the uptake of the SBA-15 support from the measured uptake.

adjacent MOP molecules.<sup>3a,4</sup> However, the MOPs confined in silica nanopores exhibit improved H<sub>2</sub> uptake. Because the H<sub>2</sub> uptake in the present study is per mole of MOP, the uptakes correlate well with the extents of dispersion of the MOPs. In samples M3S-0.1 and M3S-0.2, the MOP molecules are highly dispersed as demonstrated above, and their adsorption capacities can reach ~20 mol of H<sub>2</sub>/mol of MOP; this indicates that almost one copper site captures one H<sub>2</sub> molecule. The similar H<sub>2</sub> uptakes for M3S-0.1 and M3S-0.2 thus reflect the same extent of dispersion of the MOPs, and all of the active sites are well-exposed by dispersion of the MOP in mesoporous silica. The windows of the MOPs in the present study are ~5 Å in diameter. For the MOPs dispersed in mesoporous silica with open windows, the cavities should be accessible to other gases besides H<sub>2</sub>, such as N<sub>2</sub> and CH<sub>4</sub>. It is known that metal sites are highly dispersed in MOFs, so the H<sub>2</sub> uptake is generally large.<sup>10</sup> The H<sub>2</sub> uptakes of HKUST-1 and MIL-101, for example, are 2.2 and 1.8 mol of H<sub>2</sub>/mol of metal, respectively.<sup>10a,b</sup> Nevertheless, the adsorption capacity is also dependent on the structure as well as the metal type of the MOF. The H<sub>2</sub> uptakes of ZIF-8 and MOF-5 are 1.5 and 1.3 mol of H<sub>2</sub>/mol of metal, respectively, whereas an uptake of only 0.6 mol of H<sub>2</sub>/mol of metal is observed for PCN-13.<sup>10b-d</sup> In contrast to MOFs, the active sites in MOPs are usually blocked because of the aggregation of MOP molecules, which leads to low gas uptake. The literature concerning the adsorption of H<sub>2</sub> by MOPs is thus scarce.<sup>4b,11</sup> One iron site is reported to capture one H<sub>2</sub> molecule for IRMOF-51,<sup>11</sup> while one copper site can capture only 0.1 H<sub>2</sub> molecule for Cu<sub>4</sub>L<sub>4</sub>(DMF)<sub>4</sub>, where L denotes the ligand 3,3'-[1,3-benzenediylbis(ethynyl)]dibenzoic acid.<sup>4b</sup> As a result, the dispersion of MOP molecules provides a promising method to improve the gas adsorption capacity.

In addition to MOP 3, two other MOPs with different ligand functionality, 1 and 2, were also explored in the present study.<sup>3a,12</sup> They have geometries similar to that of MOP 3. MOP 1 is soluble in DEF, whereas MOP 2 is soluble in methanol. By the use of the same impregnation method, composites containing MOPs 1 and 2 in SBA-15 (denoted as M1S and M2S, respectively) were prepared. N<sub>2</sub> adsorption-desorption isotherms revealed that MOP 1 can be incorporated into mesopores, as evidenced by delayed hysteresis and a bimodal pore size distribution (Figure S10 in the SI). However, the constant hysteresis shape implied that MOP 2 stays outside the silica mesopores. In addition, CH<sub>2</sub>Cl<sub>2</sub>, in which none of the three MOPs is soluble, was also employed as dispersing solvent for the composite preparation. The obtained samples were denoted as M1S(CH<sub>2</sub>Cl<sub>2</sub>), M2S(CH<sub>2</sub>Cl<sub>2</sub>), and M3S(CH<sub>2</sub>Cl<sub>2</sub>), respectively. As can be seen from the N<sub>2</sub> adsorption-desorption isotherms and pore size distributions (Figure S11 in the SI), no MOP molecules could enter the mesopores of SBA-15 when CH<sub>2</sub>Cl<sub>2</sub> was used.

On the basis of the aforementioned results, two factors should be considered for the efficient incorporation of MOP molecules into silica nanopores. The first factor is the solubility of the MOPs in the solvent. A single MOP molecule already has a size of several nanometers, which is comparable to the pore size of mesoporous silica. Hence, the large steric hindrance leads to difficulty in entering the mesopores if the MOP is insoluble. Moreover, bulk MOPs prefer to aggregate as described above. If they are insoluble in the solvent, they will exist in the form of multimolecules with a size much larger than the pores of silica. In this case, it is impossible for the MOPs to enter the nanopores. The second factor is the interaction

between the MOP molecules and the surface of the mesoporous silica, which is directly related to the functional groups of the MOP molecules. This interaction is of great importance for the confinement of MOPs in mesopores. Meanwhile, the self-interaction of MOP molecules should also be taken into account, although it is difficult to elucidate. For example, MOP 2 should possess hydrogen-bonding interactions with the silica surface through its hydroxyl groups. However, MOP 2 is located outside the pores of SBA-15 despite the fact that it is soluble in methanol. The reason might be that the self-interaction of MOP molecules (probably by the coordination of hydroxyl groups with copper sites) is stronger than the interaction between the MOPs and the silica surface. These results show that the functionality of the MOP molecules plays an important role in their incorporation into mesoporous supports.

## CONCLUSION

In summary, MOP molecules have been successfully introduced into the nanopores of mesoporous silica for the first time. The solubility of the MOP and the interaction between the MOP and the silica surface play crucial roles in MOP incorporation. In comparison with bulk MOP materials in the solid state, MOPs confined in silica nanopores can be well-dispersed. As a result, the open windows and active sites in the MOPs become accessible. Our results also show that the highly dispersed MOPs exhibit obviously superior H<sub>2</sub> adsorption capacity in comparison with aggregated ones. Moreover, the thermal stability of the MOPs is enhanced after confinement in silica nanopores. The present strategy should enable various porous MOPs as well as other supramolecular architectures to be introduced into mesoporous materials with a range of pore symmetries and pore sizes, resulting in the fabrication of new types of porous composites with high potential in various applications.

## ASSOCIATED CONTENT

### Supporting Information

Experimental details; crystal structures of MOPs 1, 2, and 3; and low-angle PXRD, IR, TGA, N<sub>2</sub> adsorption, SEM, TEM, and EDX results of the composites. This material is available free of charge via the Internet at <http://pubs.acs.org>.

## AUTHOR INFORMATION

### Corresponding Author

jli@mail.chem.tamu.edu; zhou@mail.chem.tamu.edu

### Notes

The authors declare no competing financial interest.

## ACKNOWLEDGMENTS

This work was supported by the U.S. Department of Energy (DE-SC0001015, DE-FC36-07GO17033, and DE-AR0000073), the National Science Foundation (NSF CBET-0930079), and the Welch Foundation (A-1725).

## REFERENCES

- (1) (a) Yoshizawa, M.; Tamura, M.; Fujita, M. *Science* **2006**, 312, 251. (b) Northrop, B. H.; Zheng, Y.-R.; Chi, K.-W.; Stang, P. J. *Acc. Chem. Res.* **2009**, 42, 1554. (c) Pluth, M. D.; Bergman, R. G.; Raymond, K. N. *Acc. Chem. Res.* **2009**, 42, 1650. (d) Zhao, D.; Tan, S.; Yuan, D.; Lu, W.; Rezenom, Y. H.; Jiang, H.; Wang, L.-Q.; Zhou, H.-C. *Adv. Mater.* **2011**, 23, 90. (e) Li, J.-R.; Zhou, H.-C. *Angew. Chem., Int. Ed.* **2009**, 48, 8465. (f) Tranchemontagne, D. J.; Ni, Z.; O'Keeffe, M.; Yaghi, O. M. *Angew. Chem., Int. Ed.* **2008**, 47, 5136. (g) Larsen, R. W. *J. Am. Chem. Soc.* **2008**, 130, 11246. (h) Jung, M.; Kim, H.; Baek, K.; Kim, K. *Angew. Chem., Int. Ed.* **2008**, 47, 5755. (i) Dai, F.; Dou, J.; He, H.; Zhao, X.; Sun, D. *Inorg. Chem.* **2010**, 49, 4117. (j) He, Q.-T.; Li, X.-P.; Liu, Y.; Yu, Z.-Q.; Wang, W.; Su, C.-Y. *Angew. Chem., Int. Ed.* **2009**, 48, 6156.
- (2) (a) Perry, J. J., IV; Perman, J. A.; Zaworotko, M. J. *Chem. Soc. Rev.* **2009**, 38, 1400. (b) Lu, Z.; Knobler, C. B.; Furukawa, H.; Wang, B.; Liu, G.; Yaghi, O. M. *J. Am. Chem. Soc.* **2009**, 131, 12532. (c) Horcajada, P.; Chalati, T.; Serre, C.; Gillet, B.; Sebrie, C.; Baati, T.; Eubank, J. F.; Heurtaux, D.; Clayette, P.; Kreuz, C.; Chang, J.-S.; Hwang, Y. K.; Marsaud, V.; Bories, P.-N.; Cynober, L.; Gil, S.; Férey, G.; Couvreur, P.; Gref, R. *Nat. Mater.* **2010**, 9, 172. (d) Dincă, M.; Dailly, A.; Liu, Y.; Brown, C. M.; Neumann, D. A.; Long, J. R. *J. Am. Chem. Soc.* **2006**, 128, 16876. (e) Kitagawa, S.; Kitaura, R.; Noro, S.-i. *Angew. Chem., Int. Ed.* **2004**, 43, 2334. (f) Zheng, S.-T.; Wu, T.; Irfanoglu, B.; Zuo, F.; Feng, P.; Bu, X. *Angew. Chem., Int. Ed.* **2011**, 50, 8034. (g) Li, J.-R.; Timmons, D. J.; Zhou, H.-C. *J. Am. Chem. Soc.* **2009**, 131, 6368. (h) Farha, O. K.; Hupp, J. T. *Acc. Chem. Res.* **2010**, 43, 1166.
- (3) (a) Li, J.-R.; Zhou, H.-C. *Nat. Chem.* **2010**, 2, 893. (b) Lu, W.; Yuan, D.; Yakovenko, A.; Zhou, H.-C. *Chem. Commun.* **2011**, 47, 4968.
- (4) (a) Jaya Prakash, M.; Zou, Y.; Hong, S.; Park, M.; Bui, M.-P. N.; Seong, G. H.; Lah, M. S. *Inorg. Chem.* **2009**, 48, 1281. (b) Jaya Prakash, M.; Oh, M.; Liu, X.; Han, K. N.; Seong, G. H.; Lah, M. S. *Chem. Commun.* **2010**, 46, 2049.
- (5) (a) Kresge, C. T.; Leonowicz, M. E.; Roth, W. J.; Vartuli, J. C.; Beck, J. S. *Nature* **1992**, 359, 710. (b) Wan, Y.; Zhao, D. *Chem. Rev.* **2007**, 107, 2821. (c) Asefa, T.; MacLachlan, M. J.; Coombs, N.; Ozin, G. A. *Nature* **1999**, 402, 867. (d) Sayari, A.; Hamoudi, S. *Chem. Mater.* **2001**, 13, 3151. (e) Kim, S. S.; Zhang, W.; Pinnavaia, T. J. *Science* **1998**, 282, 1302.
- (6) (a) Climent, E.; Martínez-Mañez, R.; Sancenón, F.; Marcos, M. D.; Soto, J.; Maquieira, A.; Amorós, P. *Angew. Chem., Int. Ed.* **2010**, 49, 7281. (b) Coll, C.; Mondragón, L.; Martínez-Mañez, R.; Sancenón, F.; Marcos, M. D.; Soto, J.; Amorós, P.; Pérez-Payá, E. *Angew. Chem., Int. Ed.* **2011**, 50, 2138. (c) Park, C.; Kim, H.; Kim, S.; Kim, C. J. *Am. Chem. Soc.* **2009**, 131, 16614. (d) Qi, H.; Shropsowitz, K. E.; Hamad, W. Y.; MacLachlan, M. J. *J. Am. Chem. Soc.* **2011**, 133, 3728. (e) Schlossbauer, A.; Schaffert, D.; Kecht, J.; Wagner, E.; Bein, T. *J. Am. Chem. Soc.* **2008**, 130, 12558.
- (7) (a) Cozens, F. L.; Garcia, H.; Scaiano, J. C. *J. Am. Chem. Soc.* **1993**, 115, 11134. (b) Corma, A.; Díaz, U.; Ferrer, B.; Fornés, V.; Galletero, M. S.; Garcia, H. *Chem. Mater.* **2004**, 16, 1170. (c) Alvaro, M.; Chretien, M. N.; Ferrer, B.; Fornes, V.; Garcia, H.; Scaiano, J. C. *Chem. Commun.* **2001**, 2106. (d) De Vos, D. E.; Meinershagen, J. L.; Bein, T. *Angew. Chem., Int. Ed. Engl.* **1996**, 35, 2211. (e) Ozkar, S.; Ozin, G. A.; Moller, K.; Bein, T. *J. Am. Chem. Soc.* **1990**, 112, 9575. (f) De Vos, D.; Bein, T. *J. Am. Chem. Soc.* **1997**, 119, 9460. (g) Ozin, G. A.; Ozkar, S. *Chem. Mater.* **1992**, 4, 511. (h) Brühwiler, D.; Calzaferri, G. *Microporous Mesoporous Mater.* **2004**, 72, 1. (i) Huber, C.; Moller, K.; Ogunwumi, S. B.; Bein, T. *J. Phys. Chem.* **1994**, 98, 13651. (j) Huber, C.; Moller, K.; Bein, T. *Chem. Commun.* **1994**, 2619.
- (8) (a) Sun, Y.-H.; Sun, L.-B.; Li, T.-T.; Liu, X.-Q. *J. Phys. Chem. C* **2010**, 114, 18988. (b) Li, T.-T.; Sun, L.-B.; Liu, X.-Y.; Sun, Y.-H.; Song, X.-L.; Liu, X.-Q. *Chem. Commun.* **2012**, 48, 6423. (c) Zhao, D.; Feng, J.; Huo, Q.; Melosh, N.; Fredrickson, G. H.; Chmelka, B. F.; Stucky, G. D. *Science* **1998**, 279, 548.
- (9) (a) Tian, W.-H.; Sun, L.-B.; Song, X.-L.; Liu, X.-Q.; Yin, Y.; He, G.-S. *Langmuir* **2010**, 26, 17398. (b) Reichhardt, N.; Kjellman, T.; Saake, M.; Paulsen, F.; Småt, J.-H.; Lindén, M.; Alfreðsson, V. *Chem. Mater.* **2011**, 23, 3400.
- (10) (a) Krawiec, P.; Kramer, M.; Sabo, M.; Kunschke, R.; Fröde, H.; Kaskel, S. *Adv. Eng. Mater.* **2006**, 8, 293. (b) Yang, S. J.; Im, J. H.; Nishihara, H.; Jung, H.; Lee, K.; Kyotani, T.; Park, C. R. *J. Phys. Chem. C* **2012**, 116, 10529. (c) Park, K. S.; Ni, Z.; Côté, A. P.; Choi, J. Y.; Huang, R.; Uribe-Romo, F. J.; Chae, H. K.; O'Keeffe, M.; Yaghi, O. M. *Proc. Natl. Acad. Sci. U.S.A.* **2006**, 103, 10186. (d) Ma, S.; Wang, X.-S.; Collier, C. D.; Manis, E. S.; Zhou, H.-C. *Inorg. Chem.* **2007**, 46, 8499.

(11) Sudik, A. C.; Millward, A. R.; Ockwig, N. W.; Côté, A. P.; Kim, J.; Yaghi, O. M. *J. Am. Chem. Soc.* **2005**, *127*, 7110.

(12) (a) Ke, Y.; Collins, D. J.; Zhou, H.-C. *Inorg. Chem.* **2005**, *44*, 4154. (b) Abourahma, H.; Coleman, A. W.; Moulton, B.; Rather, B.; Shahgaldian, P.; Zaworotko, M. J. *Chem. Commun.* **2001**, 2380.